

${}^6\text{He} + {}^{12}\text{C}$ elastic scattering using a microscopic optical potentialV. K. Lukyanov,¹ D. N. Kadrev,² E. V. Zemlyanaya,¹ A. N. Antonov,² K. V. Lukyanov,¹ and M. K. Gaidarov²¹*Joint Institute for Nuclear Research, Dubna 141980, Russia*²*Institute for Nuclear Research and Nuclear Energy, Bulgarian Academy of Sciences, Sofia 1784, Bulgaria*

(Received 8 April 2010; published 5 August 2010)

The ${}^6\text{He} + {}^{12}\text{C}$ elastic scattering data at beam energies of 3, 38.3, and 41.6 MeV/nucleon are studied utilizing the microscopic optical potentials obtained by a double-folding procedure and also by using those inherent in the high-energy approximation. The calculated optical potentials are based on the neutron and proton density distributions of colliding nuclei established in an appropriate model for ${}^6\text{He}$ and obtained from the electron scattering form factors for ${}^{12}\text{C}$. The depths of the real and imaginary parts of the microscopic optical potentials are considered as fitting parameters. At low energy the volume optical potentials reproduce sufficiently well the experimental data. At higher energies, generally, additional surface terms having the form of a derivative of the imaginary part of the microscopic optical potential are needed. The problem of ambiguity of adjusted optical potentials is resolved requiring the respective volume integrals to obey the determined dependence on the collision energy. Estimations of the Pauli blocking effects on the optical potentials and cross sections are also given and discussed. Conclusions on the role of the aforesaid effects and on the mechanism of the considered processes are made.

DOI: [10.1103/PhysRevC.82.024604](https://doi.org/10.1103/PhysRevC.82.024604)

PACS number(s): 24.10.Ht, 25.60.-t, 21.30.-x, 21.10.Gv

I. INTRODUCTION

Experimental and theoretical studies of exotic light nuclei with a localized nuclear core and a dilute few-neutron halo or skin have been an important and advanced area in the nuclear physics in the past decades. The availability of radioactive ion beams facilities made it possible to carry out many experiments and to get more information regarding the structure of these nuclei and the respective reaction mechanisms (for more information see, e.g., the recent review of the problem in Ref. [1]). In this sense, ${}^6\text{He}$ is a typical nucleus having the weak binding energy and extended neutron halo in its periphery. The latter is the reason why in collisions with the proton and nuclear targets the projectile nucleus ${}^6\text{He}$ is breaking up with a comparably large probability that causes the flux loss in the elastic channel. Therefore, the study of elastic scattering of ${}^6\text{He}$ on protons or light targets is a powerful tool to get information on peculiarities of the mechanism of such processes.

The data on cross sections of processes with light exotic nuclei have been analyzed using various phenomenological and microscopic methods. Among the latter we should mention the microscopic analysis using the coordinate-space g -matrix folding method (e.g., Ref. [2]), as well as works where the real part of the optical potential (ReOP) is microscopically calculated (e.g., Ref. [3]) using the folding approach (e.g., Refs. [4–7]). Usually the imaginary part of the OPs (ImOP) and the spin-orbit terms have been determined phenomenologically, which has led to the usage of a number of fitting parameters. In our previous works [8,9], instead of using a phenomenological imaginary part of the OP, we have performed calculations of ${}^6\text{He} + p$ [8] and ${}^8\text{He} + p$ [9] elastic differential cross sections by means of the microscopic OP with the imaginary part taken from the OP derived in [10,11] in the frameworks of the high-energy approximation (HEA) [12–14] that is known as the Glauber theory. In the case of ${}^6\text{He} + p$ elastic scattering, it has been shown in our previous study [8] that the depth of the imaginary part of the respective

microscopically calculated OP has to be appreciably changed to get an agreement with the existing experimental data. The present study of ${}^6\text{He} + {}^{12}\text{C}$ scattering could give novel information on the mechanism of the process because of the more complicated dependence of the microscopic OP not only on the density of the projectile ${}^6\text{He}$ but also on the density of the target nucleus.

In recent years a number of works have been devoted also to the elastic scattering of ${}^6\text{He}$ on the ${}^{12}\text{C}$ nucleus and, particularly, to the study of the mechanism of this process, including the role of breakup channels. In the present article we perform an analysis of the ${}^6\text{He} + {}^{12}\text{C}$ elastic scattering data at three beam energies $E = 3$ [15], 38.3 [16], and 41.6 MeV/nucleon [17] using the microscopically calculated OP. The data have been already considered individually in the frameworks of other theoretical models. In Ref. [15] the differential cross sections at total energy 18 MeV were analyzed by means of the Woods-Saxon (WS) OP with radius parameter of the imaginary part $R_I = 5.38$ fm being about twice larger than that of the real part ($R_R = 2.4$ – 2.7 fm). The so large absorption radius in the elastic channel is thought to be caused by breakup channels that take place at the far periphery of the OP. Recently, the same ${}^6\text{He} + {}^{12}\text{C}$ elastic scattering data were fitted in Ref. [18] by the OP having a squared WS real part and a standard WS shape for its imaginary part. Furthermore, a larger radius $R_I = 6.17$ fm was obtained for the latter. The different forms of the real part of the OP and also the values of R_I in Refs. [15] and [18] just reflect the known problem of the ambiguity of parameters of phenomenological OPs when fitting them to the restricted amount of experimental data. In principle, this problem does not arise in microscopic OPs whose basic parameters have been already established by fitting to other data. In this line, a part of the problem was overcome in Ref. [16], where the elastic scattering data at $E = 38.3$ MeV/nucleon were analyzed using the semimicroscopic OP. Its real part was

defined in a double-folding model including the direct and exchange convolution integrals, whereas the imaginary part was taken phenomenologically in the WS form. Adjusting the latter to the data at relatively small angles, the reduced radius and diffuseness parameters were obtained in the range of $r_I = 1.471-1.569$ fm and $a_I = 0.358-0.524$ fm. Then, to get a better agreement at larger angles, the dynamic polarization potential (DPP) in the form of a derivative of a WS function was added to the volume OP. It affects strongly the total OP in the surface region at radii around 4–5 fm.

Recently, in Ref. [19] five Gaussian-like forms for the ${}^6\text{He}$ matter density distributions were tested using the real part of the OP without the exchange term [4] together with the five-parameter phenomenological imaginary part (volume and surface) based on the WS form. This model was adopted to study the data at 38.3 and 41.6 MeV/nucleon. Also, the authors generated another (microscopic) OP by involving in folding calculations the complex Jeukenne-Lejeune-Mahaux (JLM) effective nucleon-nucleon (NN) potential [20]. Doing so, the optimized values of the fitted parameters were fixed and then, to improve slightly the fits to data the repulsive real DPP term with two free parameters was introduced, as well. In this way, the ambiguity problem is retained just in such semi-microscopic models of OP.

In Ref. [21], an attention was paid to the dynamic polarization term in the OP. A Monte Carlo method was developed to calculate both the ${}^6\text{He}$ variational wave function and the Glauber amplitude of the microscopic scattering of the nucleons of ${}^6\text{He}$ by the nucleus ${}^{12}\text{C}$ as a whole. To this end, the phenomenological $p + {}^{12}\text{C}$ OP was utilized and, as a result, the full ${}^6\text{He} + {}^{12}\text{C}$ OP was restored from the calculated Glauber eikonal phase. Then, the difference between this OP and the single-folding OP estimated without accounting for the Glauber multiple-scattering terms, was defined as DPP responsible for the breakup channels. One can see from Fig. 5 of Ref. [21] that at 40 MeV/nucleon in the range of 4–5 fm the imaginary single-folding potential (negative) W is about 11–3 MeV and the DPP makes it deeper by about 7–3 MeV, so the full eikonal W has to be about 18–6 MeV. The certain way to investigate simultaneously the effects of elastic and breakup processes can be performed in the framework of coupled-channel (CC) methods. In Refs. [17,22] these methods have been elaborated to estimate the effects of the elastic and inelastic breakups of the projectile nucleus ${}^6\text{He} \rightarrow \alpha + n + n$ on the elastic scattering of ${}^6\text{He} + {}^{12}\text{C}$. Two models for the ${}^6\text{He}$ structure were explored in Ref. [17]. One of them uses the modified wave function from [23] of the three-body $\alpha + n + n$ system considered as a “Borromean” one. The second model constructs the α “di-neutron” potential and the corresponding two-body wave function. So far, the input potentials $U_{\alpha+n}$, $U_{\alpha+2n}$ and $U_{\alpha+{}^{12}\text{C}}$, $U_{n+{}^{12}\text{C}}$, $U_{2n+{}^{12}\text{C}}$ have been taken from the respective fits and estimations. Both of these models are completely parameter-free and explain the elastic scattering data at 41.6 MeV/nucleon fairly well. The analysis of the breakup effects of ${}^6\text{He}$ on the elastic scattering is done in Ref. [22] using the so-called continuum-discretized CC method. The reaction system is described as a four-body model of $\alpha + n + n + {}^{12}\text{C}$. The wave function of the bound and continuum states of the three-body system $\alpha + n + n$ is presented applying the

specified Gaussian expansion method, and the ground-state wave function of ${}^{12}\text{C}$ is calculated by the microscopic 3α cluster model. The resulting microscopic OP was calculated as double-folding integral with the calculated densities of ${}^6\text{He}$ and ${}^{12}\text{C}$, and then multiplied by the complex factor $(N_R + iN_I)$ with coefficients optimized by a fit to the elastic scattering data. The exchange terms in the folding OP were neglected. The results for the ${}^6\text{He} + {}^{12}\text{C}$ scattering showed that the optimum value of N_I is 0.5 at 3 MeV/nucleon and 0.3 at 38.3 MeV/nucleon, respectively, whereas $N_R = 1$. Also, it was shown that the effects of the coupling of channels are more important at comparatively large angles. The coupling smooths the diffraction structure of the differential cross sections at $E = 3$ MeV/nucleon and shifts down the corresponding curve at $E = 38.3$ MeV/nucleon calculated without coupling.

It can be mentioned that calculations by coupled reaction channel models with accounting for the cluster and continuum states are encouraged to study their sensitivity to the input information on the reaction mechanism. On the other hand, the breakup reactions reveal themselves through the dynamic polarization terms in the full OP for elastic scattering. The explicit information on these channels can be obtained from the unambiguous OP obtained from the respective analysis of the elastic scattering experimental data. In our article we try to realize the following idea. We start analyzing the elastic scattering data by the microscopic optical potential obtained in Ref. [10]. Its real part includes the direct and exchange terms that are the same used in Ref. [16]. The imaginary part of the OP is based on the Glauber theory of high-energy scattering of complex systems and is an integral which folds the nucleon-nucleon scattering amplitude f_{NN} with the density distribution functions of the bare nucleons of colliding nuclei. Therefore, first, this OP consists of parameter-free real and imaginary parts defined by the respective terms of f_{NN} . However, this potential reveals only the single-particle physical nature of the colliding nuclei because it depends on the single-particle nuclear densities. Then, we assume that additional terms to our basic OP (which have to be added to explain the experimental data) may be considered as a consequence of the presence of more complicated channels. In the case of the loosely bound ${}^6\text{He}$ projectile these terms are thought to arise from the breakup channels. Thus, the main effort should be directed to minimize the ambiguities in the fitted OPs by studying differential elastic cross sections at different energies and to involve external physical conditions to make as narrow as possible the corridor of the deviations of selected theoretical curves.

The article is organized as follows. The theoretical scheme to calculate the real and imaginary parts of the OP is given in Sec. II. The results of the calculations of OPs and the ${}^6\text{He} + {}^{12}\text{C}$ elastic scattering differential cross sections and their discussion are presented in Sec. III. The summary of the work and conclusions are given in Sec. IV.

II. THE MICROSCOPIC OPTICAL POTENTIAL

Here, we give the main expressions for the real and imaginary parts of the nucleus-nucleus OP,

$$U(r) = V^{\text{DF}}(r) + iW(r). \quad (1)$$

The real part V^{DF} consists of the direct and exchange double-folding (DF) integrals that include an effective NN potential and density distribution functions of colliding nuclei:

$$V^{\text{DF}}(r) = V^D(r) + V^{\text{EX}}(r). \quad (2)$$

The formalism of the DF potentials is described in details (e.g., in Refs. [4,6]). In general, in Eq. (2) V^D and V^{EX} are composed from the isoscalar (IS) and isovector (IV) contributions, but in the considered case the isovector part is omitted because $Z = N$ in the target nucleus ${}^{12}\text{C}$ and, thus, one can write:

$$V^D(r) = \int d^3r_p d^3r_t \rho_p(\mathbf{r}_p) \rho_t(\mathbf{r}_t) v_{NN}^D(s), \quad (3)$$

$$V^{\text{EX}}(r) = \int d^3r_p d^3r_t \rho_p(\mathbf{r}_p, \mathbf{r}_p + \mathbf{s}) \rho_t(\mathbf{r}_t, \mathbf{r}_t - \mathbf{s}) \times v_{NN}^{\text{EX}}(s) \exp\left[\frac{i\mathbf{K}(r) \cdot \mathbf{s}}{M}\right], \quad (4)$$

where $\mathbf{s} = \mathbf{r} + \mathbf{r}_t - \mathbf{r}_p$ is the vector between two nucleons, one of which belongs to the projectile and another one to the target nucleus. In Eq. (3) $\rho_p(\mathbf{r}_p)$ and $\rho_t(\mathbf{r}_t)$ are the densities of the projectile and the target, respectively. In Eq. (4) $\rho_p(\mathbf{r}_p, \mathbf{r}_p + \mathbf{s})$ and $\rho_t(\mathbf{r}_t, \mathbf{r}_t - \mathbf{s})$ are the density matrices for the projectile and the target that are usually taken in an approximate form [24]. In the modern calculations of the DF potentials the effective interaction v_{NN}^D (of CDM3Y6-type) based on the Paris NN forces and having the form,

$$v_{NN}^D(E, \rho, s) = g(E)F(\rho)v(s), \quad (5)$$

is usually applied with the distance dependence given by

$$v(s) = \sum_{i=1}^3 N_i \frac{\exp(-\mu_i s)}{\mu_i s}, \quad (6)$$

and with terms of the energy and density dependencies:

$$g(E) = 1 - 0.003E, \quad F(\rho) = C[1 + \alpha e^{-\beta\rho} - \gamma\rho]. \quad (7)$$

The energy-dependent factor in Eq. (7) is taken to be a linear function of the bombarding energy per nucleon, whereas ρ in $F(\rho)$ is the sum of the projectile and target densities, $\rho = \rho_p + \rho_t$. The parameters N_i, μ_i [Eq. (6)], C, α, β, γ [Eq. (7)], and all details of the mathematical treatments and calculations are given in Refs. [6,25].

In Eq. (4) v_{NN}^{EX} is the exchange part of the effective NN interaction. It is important to note that the energy dependence of V^{EX} arises primarily from the contribution of the exponent in the integrand of Eq. (4). Indeed, there the local nucleus-nucleus momentum

$$K(r) = \left\{ \frac{2Mm}{\hbar^2} [E - V^{\text{DF}}(r) - V_c(r)] \right\}^{1/2}, \quad (8)$$

with A_p, A_t, m being the projectile and target atomic numbers and the nucleon mass, and $M = A_p A_t / (A_p + A_t)$. As can be seen, $K(r)$ depends on the folding potential $V^{\text{DF}}(r)$ that has to be calculated itself and, therefore, we have to deal with a typical nonlinear problem. Usually, two different kinds of effective NN potentials are employed in calculations, namely the Paris CDM3Y6 and the Reid DDM3Y1 NN interactions, which are defined by two different sets of the aforementioned

parameters. The direct parts of these potentials have different signs and, for example, in the case of CDM3Y6 forces the V^{EX} is negative whereas V^D is positive. So, if in the calculations one takes only the direct part of V^{DF} with the Paris M3Y NN forces, then the corresponding real part of such an OP is a positive one. Therefore, one should proceed carefully when neglecting the exchange part of the OP.

Concerning the imaginary part of our OP, we take it in two forms. In the first case the imaginary part has the same form as the real one but with different strength. At the same time, we test another shape of the imaginary part that corresponds to the full microscopic OP derived in Refs. [10,11] within the HEA [12,13]. In the momentum representation this OP has the form,

$$U_{\text{opt}}^H(r) = -\frac{E}{k} \bar{\sigma}_N (i + \bar{\alpha}_N) \frac{1}{(2\pi)^3} \times \int e^{-i\mathbf{q}\mathbf{r}} \rho_p(q) \rho_t(q) f_N(q) d^3q. \quad (9)$$

Here, $\bar{\sigma}_N$ and $\bar{\alpha}_N$ are the averaged over isospins of nuclei, the NN total scattering cross section and the ratio of real to imaginary parts of the forward NN amplitude, both being parameterized (e.g., in Refs. [26,27]). The NN form factor is taken as $f_N(q) = \exp(-q^2\beta/2)$ with the slope parameter $\beta = 0.219 \text{ fm}^2$ [28]. It is easy to verify that the eikonal phase for this potential,

$$\Phi(b) = -\frac{1}{\hbar v} \int_{-\infty}^{\infty} U_{\text{opt}}^H(\sqrt{b^2 + z^2}) dz, \quad (10)$$

is reduced to the HEA microscopic phase Φ_N for nucleus-nucleus scattering. To this end, let us substitute Eq. (9) in Eq. (10) and simplify the latter in the cylindrical coordinate system, where $d^3q = q_{\perp} dq_{\perp} d\phi dq_{\parallel}$ and $\mathbf{q}\mathbf{r} = q_{\perp} b \cos\phi + q_{\parallel} z$, $q^2 = q_{\perp}^2 + q_{\parallel}^2$, $q_{\perp} = q \cos(\vartheta/2)$, $q_{\parallel} = q \sin(\vartheta/2)$. Here, ϑ is the angle of scattering and b is the impact parameter of the projectile trajectory of motion directed straight ahead along the z axis. In HEA one neglects the longitudinal part of the transfer momentum $q_{\parallel} \ll q_{\perp}$ and the small angle terms $q_{\parallel} z \simeq q_{\parallel} 2R \simeq kR\vartheta^2 \ll 1$ to give $q \simeq q_{\perp}$ at $\vartheta \ll \sqrt{1/kR}$. Therefore, the smooth functions become $\rho(q) \rightarrow \rho(q_{\perp})$, and $f_N(q) \rightarrow f_N(q_{\perp})$, and then one can perform integrations $\int_{-\infty}^{\infty} dq_{\parallel} \exp(-iq_{\parallel} z) = 2\pi\delta(z)$ and $\int_0^{2\pi} d\phi \exp(-iq_{\perp} b \cos\phi) = 2\pi J_0(q_{\perp} b)$. Thus, as a result we obtain the standard form of the HEA phase in the so-called optical limit of the Glauber theory:

$$\Phi_N(b) = \frac{1}{4\pi} \bar{\sigma}_N (i + \bar{\alpha}_N) \int_0^{\infty} J_0(qb) \rho_p(q) \rho_t(q) f_N(q) q dq. \quad (11)$$

Here, one sets $q_{\perp} = q = 2k \sin(\vartheta/2)$ that is valid at small angles of scattering $\vartheta \ll \sqrt{1/kR}$.

As a rule this phase is employed to estimate the HEA elastic scattering amplitude,

$$f(\vartheta) = ik \int_0^{\infty} J_0(qb) [1 - e^{i\Phi_N(b)}] b db. \quad (12)$$

In applications of $f(\vartheta)$ from Eq. (12) the main limitations $E \gg |U|$ and $\vartheta \ll \sqrt{1/kR}$ are connected with the basic

assumption that the integration in Eqs. (10)–(12) is performed along the z axis with a straight-line classical trajectory of motion. To correct partly this approximation at lower energies and larger angles one can take into account the trajectory distortion. For the Coulomb distortion, the respective prescription was used (e.g., in Ref. [29]), where the impact parameter b in (12) was replaced by $b_c = \bar{a} + \sqrt{\bar{a}^2 + b^2}$ with $\bar{a} = Z_1 Z_2 e^2 / 2E_{\text{c.m.}}$ being the half-distance of closest approach in the Coulomb field of a point charge. The approximated method for the inclusion of a distortion in the presence of a nuclear potential was formulated (e.g., in Ref. [30]). However, all these attempts cannot fully account for the distortion effects of the classical trajectory caused by the total complex OP. Instead, the conventional way to resolve this problem is to compute numerically the Schrödinger equation with the initial OP given by Eq. (9). Moreover, when using this original OP in the wave equation, it becomes not necessary to neglect the longitudinal terms in the momentum transfer. In this way, one expects that the initial OP (9) can be used not only for the scattering at high energies but also for comparably lower energies and for a wider range of scattering angles.

Hereafter, we shall use only the imaginary part of the full OP (9) transformed [by using the equality $\int d\Omega_q \exp(-i\mathbf{q}\mathbf{r}) = 4\pi j_0(qr)$] to the form,

$$W^H(r) = -\frac{1}{2\pi^2} \frac{E}{k} \bar{\sigma}_N \int_0^\infty j_0(qr) \rho_p(q) \rho_t(q) f_N(q) q^2 dq. \quad (13)$$

In the further calculations the microscopic volume optical potential has the following form:

$$U(r) = N_R V^{\text{DF}}(r) + iN_I W(r), \quad (14)$$

where $W(r)$ is taken to be equal either to $V^{\text{DF}}(r)$ or to $W^H(r)$. The parameters N_R and N_I entering Eq. (14) renormalize the strength of the OP and are fitted by comparison with the experimental cross sections. In the present work, attempting to simulate the surface effects caused by the polarization potential [31–33], we add to the volume potential [Eq. (14)] the respective surface terms. Usually, they are taken as a derivative of the imaginary part of the OP, as follows:

$$W^{\text{sf}}(r) = -iN_I^{\text{sf}} \frac{dW(r)}{dr}, \quad (15)$$

$$= -iN_I^{\text{sf}} r \frac{dW(r)}{dr}, \quad (16)$$

$$= -iN_I^{\text{sf}} r^2 \frac{dW(r)}{dr}, \quad (17)$$

$$= -iN_I^{\text{sf}} \frac{dW(r-\delta)}{dr}, \quad (18)$$

where N_I^{sf} is also a fitting parameter, δ gives the shift of the potential (18), and in our case is fixed to be $\delta = 1$ fm.

Concluding this section, we would like to emphasize that our basic OP contains the same real part as that one in Ref. [16], but instead of the phenomenological ImOP, we utilize a microscopically calculated imaginary potential. In addition, in contrast to Ref. [19] where only the direct part of the ReOP and a part of the ImOP were calculated microscopically, in the present work we include also the microscopic

exchange part of the OP. Concerning the comparison with the experimental data, we consider not only selected data (as, e.g., at $E = 38.3$ MeV/nucleon in [16], and at $E = 38.3$ and 41.6 MeV/nucleon in [19]) but add also the data at fairly low energy $E = 3$ MeV/nucleon and analyze simultaneously the three sets of data. This allows us to determine the ambiguities when adjusting the values of the OP parameters [Eqs. (14)–(18)] because we include an additional condition in the fitting procedure. Namely, we consider also the energy behavior of the volume integrals of ReOP and ImOP as an additional physical constraint. In this way, the information on the dynamical polarization potentials obtained from a more precise analysis can be considered as more reliable.

III. RESULTS AND DISCUSSION

In this section, we present the results of the calculations of the microscopic OPs and the respective elastic scattering differential cross sections at energies $E < 100$ MeV/nucleon obtained following the theoretical scheme in Sec. II. In contrast to the cases of ${}^6,8\text{He} + p$ elastic scattering where only the density of the projectile ${}^6,8\text{He}$ takes part in the calculations, in our case both densities, of the projectile ${}^6\text{He}$ and the target ${}^{12}\text{C}$, have to be included in the calculations of the OP [see Eqs. (3) and (4)]. The results of our work [8] on the ${}^6\text{He} + p$ elastic scattering at $E < 100$ MeV/nucleon showed that the large-scale shell model (LSSM) density of ${}^6\text{He}$ microscopically calculated in Ref. [7] using a complete $4\hbar\omega$ shell-model space and the Woods-Saxon single-particle wave function basis with realistic exponential asymptotic behavior is the most preferable one and it is used also in the present work. For ${}^{12}\text{C}$ we use the symmetrized Fermi-type density with the radius and diffuseness parameters $c = 3.593$ fm and $a = 0.493$ fm from Ref. [34]. They were obtained by defolding the ${}^{12}\text{C}$ charge density distribution deduced in Ref. [35] from analysis of the corresponding electron scattering form factors.

In Fig. 1 are shown the densities of ${}^6\text{He}$ and ${}^{12}\text{C}$, as well as the OPs V^{DF} calculated using Eqs. (1)–(7) and W^H obtained within the HEA [Eq. (13)] for the three cases of the incident energy that are considered ($E = 3, 38.3$ and 41.6 MeV/nucleon). It can be seen that the increase of the energy leads to reduced depths and slopes of ReOP and ImOP.

We calculated the ${}^6\text{He} + {}^{12}\text{C}$ elastic scattering differential cross sections using the program DWUCK4 [36] and the microscopically calculated OP [Eq. (14)]. As already mentioned in Sec. II, in the calculations we add to these volume potentials the respective surface terms [Eqs. (15)–(18)]. The latter is done only for the ImOP, having in mind that because of the breakup channel effects there is a “loss of the flux” from the elastic channel. We note that for the ${}^6\text{He} + {}^{12}\text{C}$ process there is not a spin-orbit contribution to the OP in contrast to the ${}^6,8\text{He} + p$ cases.

In our work we consider the set of the N_i coefficients (N_R , N_I , and N_I^{sf}) as parameters to be found out from the comparison with the empirical data. We should mention (as it had been emphasized in our previous works [8,9] for ${}^6,8\text{He} + p$ scattering) that we do not aim to find a complete agreement

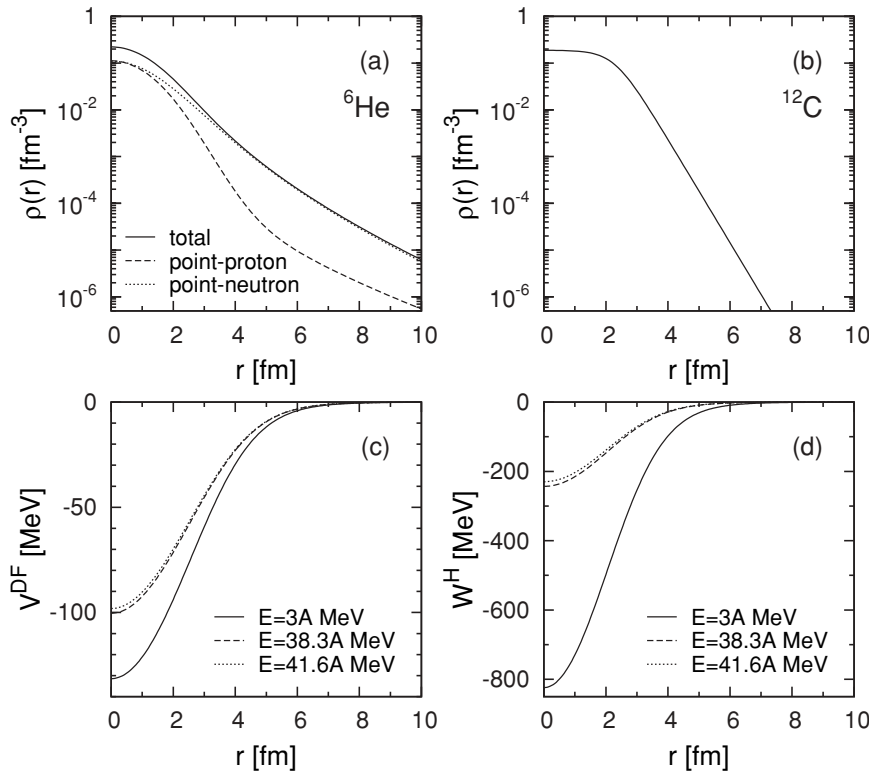


FIG. 1. (Top) Total, point-proton and point-neutron microscopic LSSM densities of ${}^6\text{He}$ (from Ref. [7]) (a) and the density of ${}^{12}\text{C}$ [34,35] (b). (Bottom) Microscopic OPs V^{DF} (c) and W^{H} (d) for the ${}^6\text{He} + {}^{12}\text{C}$ elastic scattering at $E = 3, 38.3$ and 41.6 MeV/nucleon ($N_R = N_I = 1$ and $N_I^{\text{sf}} = 0$).

with the data. The introduction of the N 's related to the depths of the different components of the OPs can be considered as a way to introduce a quantitative measure of the deviations of the predictions of our method from the reality (e.g., the differences of N 's from unity for given energies).

The starting energy of our calculations was $E = 38.3$ MeV/nucleon. At this energy HEA can be applied as a good approximation to calculate the ImOP. As a first example, we present in Fig. 2 the results of our calculations using: (i) only volume OP (14) for the two types of ImOP (V^{DF} and W^{H}) and (ii) different forms of the surface contributions to the ImOP [Eqs. (15)–(18)]. The N parameters are determined by a fitting procedure. The results of the calculations are close

to each other and that is why all of them are presented inside a gray area. Two definitions of χ^2 are used:

$$\chi^2 = \frac{1}{N} \sum_{i=1}^N \left[\frac{\sigma^{\text{exp}}(\vartheta_i) - \sigma^{\text{th}}(\vartheta_i)}{\Delta\sigma^{\text{exp}}(\vartheta_i)} \right]^2, \quad (19)$$

$$\chi_\sigma^2 = \frac{1}{N} \sum_{i=1}^N \frac{[\sigma^{\text{exp}}(\vartheta_i) - \sigma^{\text{th}}(\vartheta_i)]^2}{\sigma^{\text{th}}(\vartheta_i)}. \quad (20)$$

In the first definition the χ^2 values were obtained considering uniform 10% errors for all the analyzed data. This procedure is often used by other authors. Here, $\sigma^{\text{th}}(\vartheta_i)$ and $\sigma^{\text{exp}}(\vartheta_i)$ are the theoretical and experimental values of the differential cross sections ($d\sigma/d\Omega$) or their ratio to the Rutherford cross section. In the last case the χ_σ^2 is dimensionless and its values for the results in Fig. 2 range in the interval $0.191 \leq \chi_\sigma^2 \leq 0.362$, whereas the values of N_R are in the interval $0.893 \leq N_R \leq 1.268$. The values of the predicted total reaction cross section σ_R are also calculated.

One can see from Fig. 2 that the inclusion of different forms of the surface potential leads to almost similar results for the cross section. This was also the case of ${}^8\text{He} + p$ processes studied in our previous work [9]. As is known, the problem of the ambiguity of the N values arises when the fitting procedure concerns a limited number of experimental data.

The situation is ambiguous also for the case of the energy $E = 41.6$ MeV/nucleon.

The case of $E = 3$ MeV/nucleon is a particular one because of this rather low energy. Nevertheless, we made an attempt to consider it using OP obtained in our method. The calculations showed that for this energy the fitting procedure led to $N_I^{\text{sf}} = 0$ for the case of the surface term given by Eq. (16). We note

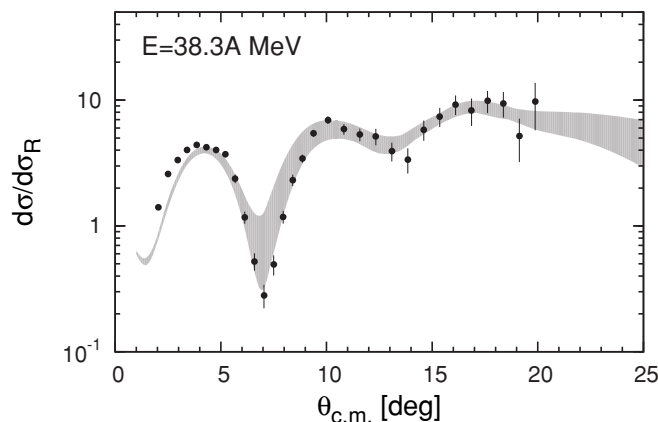


FIG. 2. Cross sections of ${}^6\text{He} + {}^{12}\text{C}$ elastic scattering at $E = 38.3$ MeV/nucleon calculated by fitting the $N_R, N_I, N_I^{\text{sf}}$ parameters of the microscopic OP [Eqs. (14)–(18)] (gray area). The experimental data are taken from Ref. [16].

TABLE I. The optimal values of the parameters N_R , N_I for the volume OP [Eq. (14)] for the elastic ${}^6\text{He} + {}^{12}\text{C}$ cross sections at energies $E = 3, 38.3, \text{ and } 41.6$ MeV/nucleon when the imaginary potential W was selected in the forms W^H or V^{DF} . The values of the volume integrals J_V and J_W , χ^2 , and total reaction cross sections σ_R (in mb) are also given.

E	W	N_R	N_I	J_V	J_W	χ^2	σ_R
3	W^H	0.826	0.154	297.109	212.952	9.121	1427.33
3	V^{DF}	0.793	0.345	285.239	124.095	9.890	1428.52
38.3	W^H	1.268	0.511	353.442	208.567	80.808	1028.77
38.3	V^{DF}	1.123	0.472	313.025	131.565	50.847	1033.79
41.6	W^H	0.897	0.689	244.933	265.680	3.737	1067.32
41.6	V^{DF}	0.814	0.584	222.269	159.466	3.774	1067.55

that in the case of $E = 3$ MeV/nucleon the ambiguity in the explanation of the data [15] still remains.

In what follows, we tried to choose the most physical values of N 's for the energies considered. As is known, the fitting procedure belongs to the class of the ill-posed problems (e.g., Ref. [37]). To resolve this problem it is necessary to impose some physical constraints when fitting the parameters of a model. In our case it might be the data on the total cross sections but often the corresponding values are missing. Another physical criterion that has to be imposed is the obtained potentials to obey a determined behavior of the volume integrals [4],

$$J_V = -\frac{4\pi}{A_p A_t} \int N_R V^{\text{DF}}(r) r^2 dr, \quad (21)$$

$$J_W = -\frac{4\pi}{A_p A_t} \int N_I W(r) r^2 dr, \quad (22)$$

as functions of the energy. Indeed, it was shown for nucleon and light-ions scattering on nuclei (see, e.g., Refs. [38–40]) that the values of the volume integrals J_V decrease with the energy increase at $E < 100$ MeV/nucleon, whereas J_W increases at low energies up to 10–20 MeV/nucleon and then saturates. We would like to note that such conditions were also imposed in Ref. [9] when the microscopic OPs were introduced to study the ${}^8\text{He} + p$ scattering and their depth parameters N_R and N_I were fitted. The values of J_V and J_W for the ${}^6\text{He} + {}^{12}\text{C}$ scattering that fulfill the condition for their energy dependence are presented in Tables I–III. In the cases when we include surface terms to the ImOP we modify J_W accounting for them.

In the next part of the work we select those sets of the N parameters that lead to the already mentioned behavior of J_V and J_W as functions of the energy for three cases: (1) only the volume terms; (2) the volume terms plus the surface term given

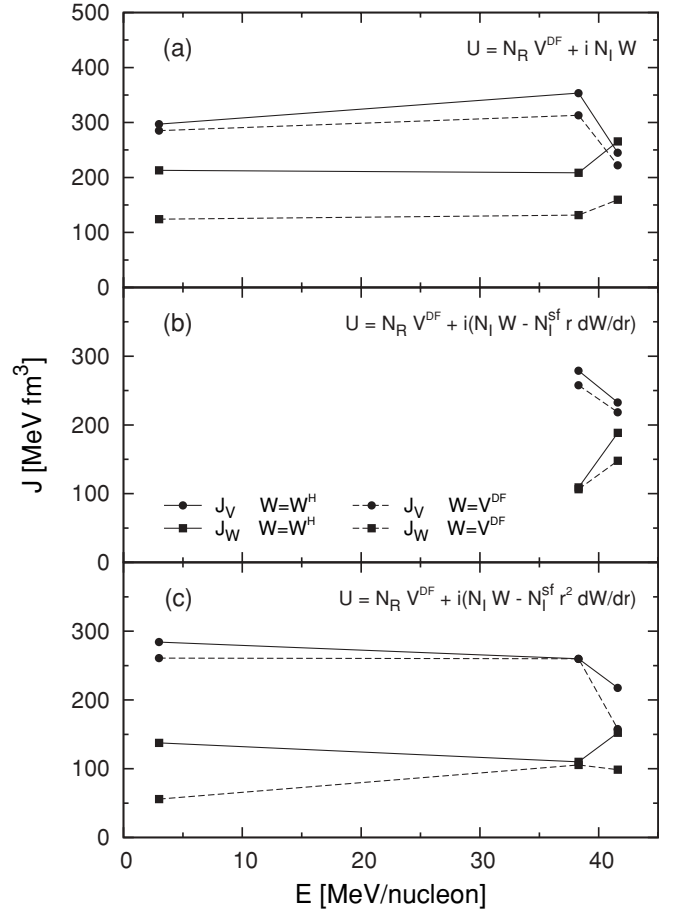


FIG. 3. The energy dependence of the volume integrals J_V and J_W that are related to the selected OPs from a number of fitted microscopic OPs with and without surface terms. The values of N 's, J_V , J_W , χ^2 , and σ_R corresponding to the symbols in panels (a)–(c) are given in Tables I–III, respectively.

by Eq. (16); (3) the volume terms plus the surface term from Eq. (17). The behavior of the volume integrals as functions of the energy is presented in Fig. 3.

Using the same values of the N parameters already selected, we present in Figs. 4–6 the cross sections for the three energies and for the three cases mentioned previously. One can see that the best agreement with the data for all the three energies can be obtained by the OP with the volume and surface term [Eq. (17)] whose volume integrals follow (though approximately) the already mentioned energy dependence.

In Figs. 7(a) and 7(b) are given those microscopic ReOP and ImOP that lead to the best agreement with the experimental data for the ${}^6\text{He} + {}^{12}\text{C}$ elastic scattering cross sections shown

TABLE II. The same as Table I but for the parameters N_R , N_I , and N_I^{sf} of the total OP with the surface term from Eq. (16).

E	W	N_R	N_I	N_I^{sf}	J_V	J_W	χ^2	σ_R
38.3	W^H	1.000	0.023	0.082	278.740	109.172	17.399	1055.67
38.3	V^{DF}	0.924	0.082	0.101	257.556	106.420	5.006	1174.66
41.6	W^H	0.852	0.337	0.051	232.645	188.590	3.734	1070.77
41.6	V^{DF}	0.800	0.500	0.014	218.446	147.876	3.781	1072.40

TABLE III. The same as Table I but for the parameters N_R , N_I , and N_I^{sf} of the total OP with the surface term from Eq. (17). The values of N_I^{sf} are in fm^{-1} .

E	W	N_R	N_I	N_I^{sf}	J_V	J_W	χ^2	σ_R
3	W^H	0.790	0.074	0.002	284.160	137.506	8.912	1449.98
3	V^{DF}	0.725	0.040	0.008	260.779	55.924	9.418	1533.22
38.3	W^H	0.932	0.028	0.019	259.786	110.017	5.059	1185.22
38.3	V^{DF}	0.932	0.204	0.012	259.786	105.469	8.425	1161.91
41.6	W^H	0.797	0.255	0.011	217.627	152.281	3.711	1091.46
41.6	V^{DF}	0.578	0.041	0.022	157.827	98.546	2.398	1224.91

in Figs. 4–6 for energies $E = 3, 38.3$ and 41.6 MeV/nucleon. For $E = 3$ MeV/nucleon there are only volume OPs, whereas for $E = 38.3$ MeV/nucleon there is a surface contribution to the ImOP using $W = V^{\text{DF}}$ in Eq. (16) and $W = W^H$ in Eq. (17); for $E = 41.6$ MeV/nucleon there are only volume OPs.

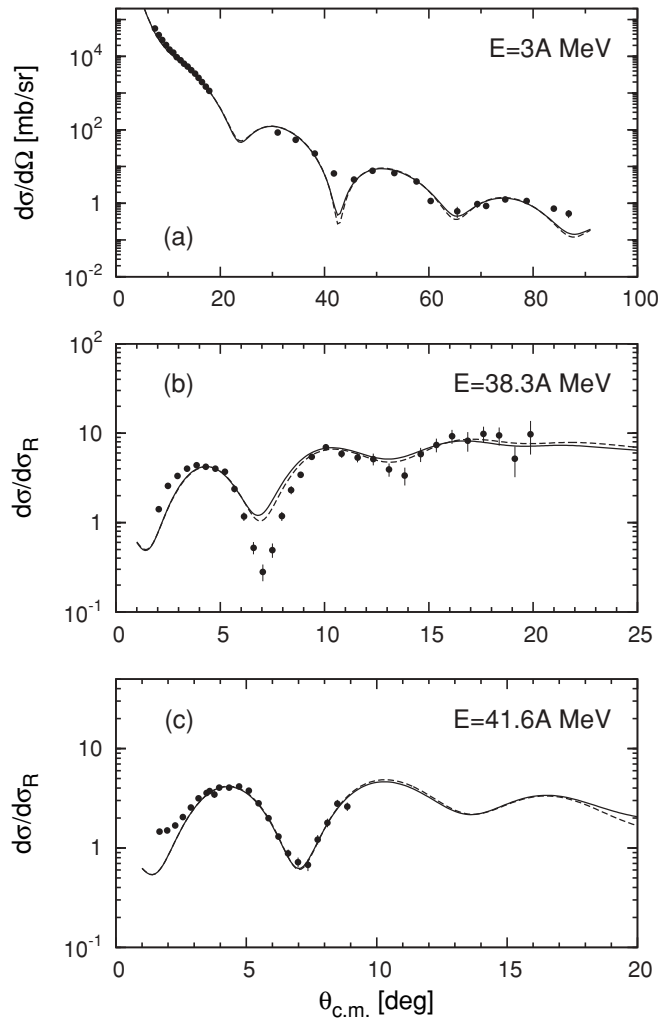


FIG. 4. Differential cross section of elastic ${}^6\text{He} + {}^{12}\text{C}$ scattering at $E = 3$ (a), 38.3 (b), and 41.6 MeV/nucleon (c) calculated using only volume OP [Eq. (14)]. Solid line, $W = W^H$; dashed line, $W = V^{\text{DF}}$. The values of the fitted parameters N_R and N_I corresponding to the curves in the top, middle, and bottom part are given in Table I. The experimental data are taken from Refs. [15–17].

In Figs. 8(b) and 8(c) the real and imaginary parts of the OP for $E = 3$ MeV/nucleon obtained in the present work are compared with the phenomenological OPs from Ref. [15] (where WS forms have been used for ReOP and ImOP) and from Ref. [18] (with the OP having a squared WS real part and a standard WS shape for the ImOP). The results for the cross sections are shown in Fig. 8(a). One can see much better agreement for our cross sections obtained using microscopic OPs than those obtained in a phenomenological way in Refs. [15,18].

We should note also that in Ref. [18] the ReOP (V_0) increases and the ImOP (W_0) decreases with the energy increase, which is in contradiction with the generally accepted results and with the behavior of the volume integrals as functions of the energy [38–40].

In Fig. 9 the deviations of the OPs from their volume parts are presented for the three energies considered. In our

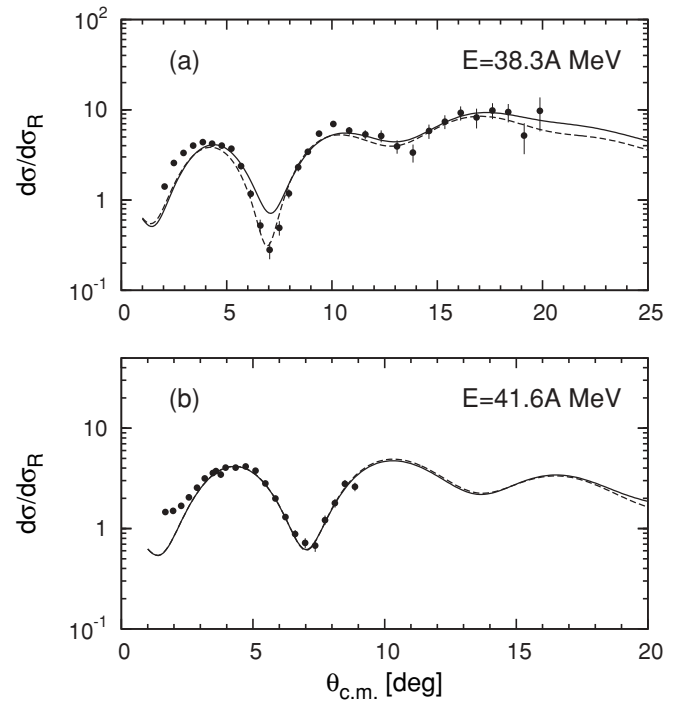


FIG. 5. The same as in Fig. 4 (without the case for $E = 3$ MeV/nucleon) at $E = 38.3$ (a) and $E = 41.6$ MeV/nucleon (b) calculated using volume OP and surface contribution to the ImOP [Eq. (16)]. The values of the N parameters are given in Table II. The experimental data are taken from Refs. [16,17].

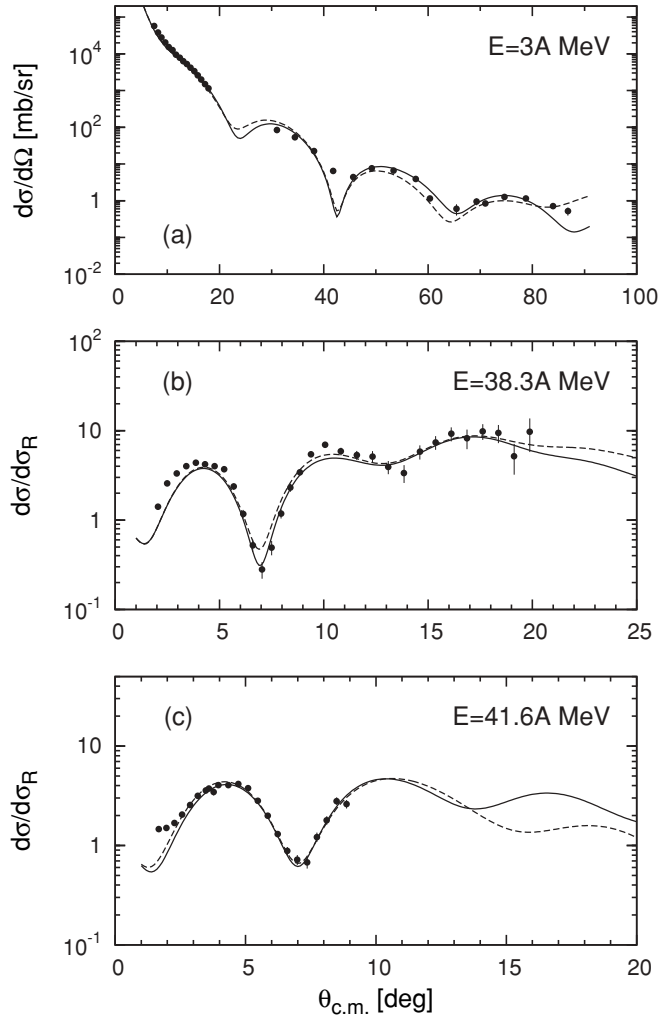


FIG. 6. The same as in Fig. 4 but for the volume OP and surface contribution to the ImOP [Eq. (17)]. The corresponding N 's are given in Table III. The experimental data are taken from Refs. [15–17].

theoretical scheme they are related to the surface parts of the ImOP in the form of $N_I^{sf} r dW^{H(DF)}/dr$ and $N_I^{sf} r^2 dW^{(H)DF}/dr$. As is known, these contributions can be considered as the so-called dynamical polarization potential that owes its origin to effects of the breakup of a pair of neutrons from ${}^6\text{He}$.

In what follows, we would like to discuss the deviations of the values of the coefficients N 's (and, particularly, of N_I) from unity. As known, a folding model can be thought as meaningful only when the renormalization coefficients of the folded potential are close to unity. In our case (see Table I) $N_I = 0.154$ for $E = 3$ MeV/nucleon and $N_I = 0.689$ for $E = 41.6$ MeV/nucleon. Here, we would like to emphasize that the obtained values of N_I within the HEA for the small energy $E = 3$ MeV/nucleon reflect the effects of Pauli blocking (see, e.g., [41]) that in the case of nucleus-nucleus scattering reduce the depth of ImOP by a factor of 10 or more. This is related to the fact that in the HEA the microscopic optical potential is proportional to the free NN cross section (σ_N), that in nuclear matter is reduced by the so-called in-medium factor f_m that

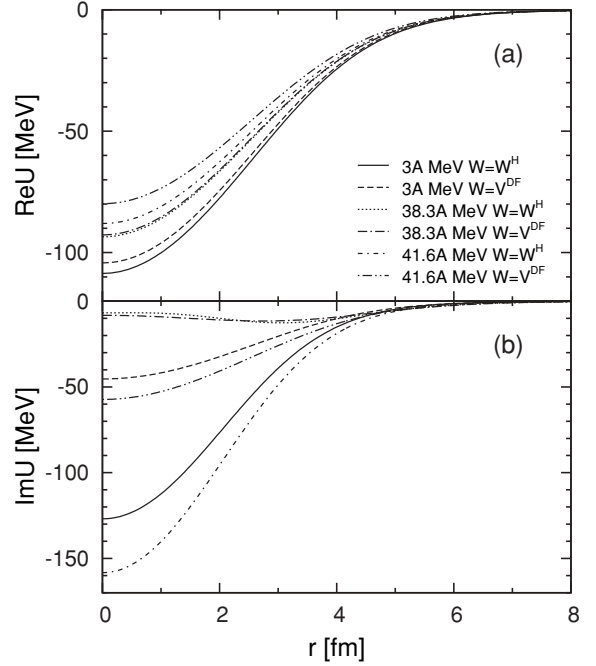


FIG. 7. Selected OPs that lead to best agreement with the data of the ${}^6\text{He} + {}^{12}\text{C}$ cross sections shown in Figs. 4–6. The values of the N parameters for the curves at $E = 3$ and 41.6 MeV/nucleon (with $W = W^H$ and $W = V^{DF}$) are listed in Table I, whereas the values at $E = 38.3$ MeV/nucleon are given in Table II for $W = V^{DF}$ and Table III for $W = W^H$.

accounts for, in particular, the Pauli blocking effect:

$$\sigma_N^{(m)} = \sigma_N f_m. \quad (23)$$

There are many estimations of the factor f_m , for example, those based in the Brückner-Hartree-Fock (BHF) theory [42–44]. In Ref. [43] the expression for f_m is obtained by a least-squares fit to the experimental total reaction cross-section data over a wide incident energy range. The latter gives the separate forms for the σ_{pp} and σ_{pn} cross sections accompanied by the factors,

$$f_m(np) = \frac{1 + 20.88E^{0.04}\rho^{2.02}}{1 + 35.86\rho^{1.90}}, \quad (24)$$

$$f_m(nn) = \frac{1 + 7.772E^{0.06}\rho^{1.48}}{1 + 18.01\rho^{1.46}}, \quad (25)$$

where E is the kinetic energy in laboratory system per nucleon of the projectile nucleus, and $\rho = \rho_p + \rho_t$. [One can guess that in Eqs. (24) and (25) the numerical coefficients in the second terms of f_m have the respective dimensions to measure E_{lab} in MeV and ρ in fm^{-3}]. Recently, expressions for f_m were presented in Ref. [44] in the approximation of the isotropic free NN cross section. In this approach the Pauli projection operator in the g -matrix as a solution of the Bethe-Goldstone equation is considered as a geometrical factor that restricts the conditions on the available angles of scattering of the NN pair to unoccupied final states. The result for the NN correction

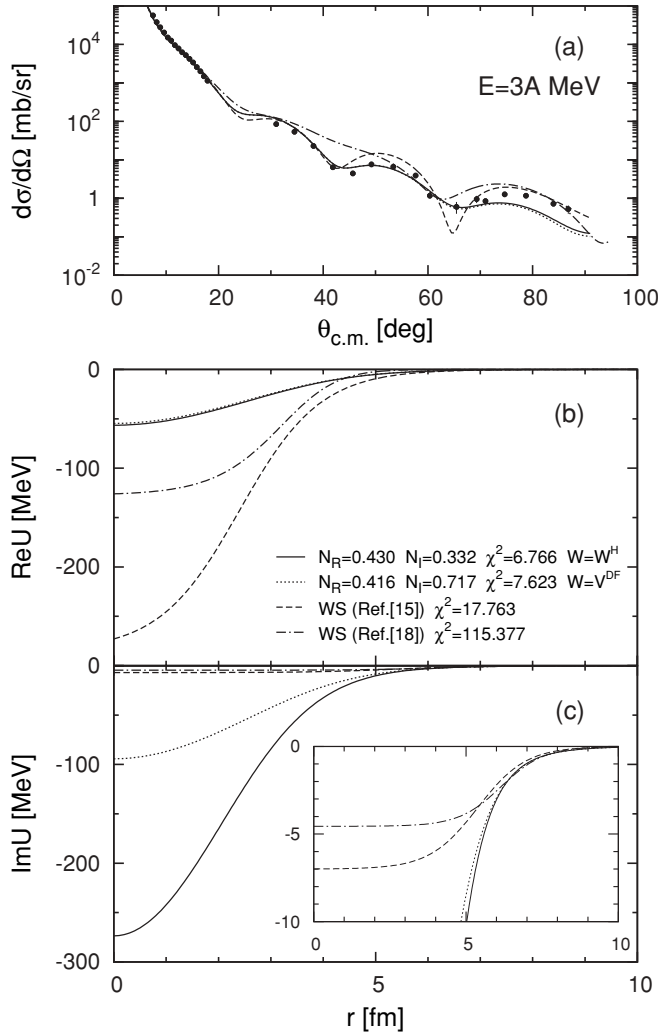


FIG. 8. (a) Differential cross section of elastic ${}^6\text{He} + {}^{12}\text{C}$ scattering at $E = 3$ MeV/nucleon. Solid and dotted lines show the results with microscopic ImOP W^H and V^{DF} , respectively. The results with the phenomenological OPs from Refs. [15] and [18] are given by dashed and dash-dotted lines, correspondingly. The experimental data are taken from Ref. [15]. The ReOP and ImOP for $E = 3$ MeV/nucleon microscopically obtained in the present work and those from Refs. [15] and [18] are given in (b) and (c), respectively.

factor is in the form [44]:

$$f_m = \frac{1}{1 + 1.892 \left(\frac{|\rho_p - \rho_t|}{\bar{\rho}\rho_0} \right)^{2.75}} f(E), \quad (26)$$

where

$$f(E > 46.27\bar{\rho}^{2/3}) = 1 - \frac{37.02}{E}, \quad (27)$$

$$f(E < 46.27\bar{\rho}^{2/3}) = \frac{E}{231.38\bar{\rho}^{2/3}}. \quad (28)$$

E is the laboratory energy per nucleon in MeV, $\rho_0 = 0.17 \text{ fm}^{-3}$, and $\bar{\rho} = (\rho_p + \rho_t)/\rho_0$. In practice, hard numerical problems arise when one intends to use these formulas in calculations of folding integrals for the microscopic potentials.

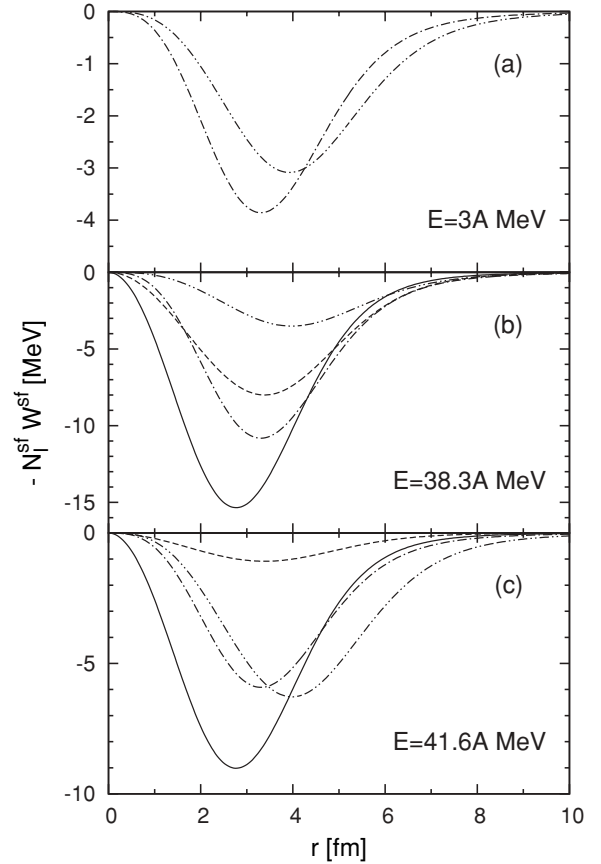


FIG. 9. The surface ImOPs (dynamical polarization OPs) used in the calculations of the cross sections of ${}^6\text{He} + {}^{12}\text{C}$ elastic scattering at $E = 3$ (a), 38.3 (b), and 41.6 MeV/nucleon (c). Solid and dashed lines, using Eq. (16) with N values of from Table II and with $W = W^H$ and $W = V^{DF}$, respectively; dot-dashed and dashed two-dot lines, using Eq. (17) with N 's from Table III and with $W = W^H$ and $W = V^{DF}$, respectively.

Instead, it is easy to estimate the in-medium effects in the realistic case suggesting that the main contribution comes from the region of half-density radii of the colliding nuclei, where $\rho = \rho_p + \rho_t = \rho_0$, $\rho_p - \rho_t = 0$, and $\bar{\rho} = 1$. Then, the first term in Eq. (26) equals to 1, and thus one gets $f(E) \simeq 0.013$ for $E = 3$ MeV/nucleon and $f(E) \simeq 0.18$ for $E = 41.6$ MeV/nucleon. The use of Eqs. (24) and (25) (from [43]) lead to the following estimations: $f_m(np) = 0.717$ and $f_m(nn) = 0.68$ for $E = 3$ MeV/nucleon and $f_m(np) = 0.75$ and $f_m(nn) = 0.74$ for $E = 41.6$ MeV/nucleon. One can see that the results for $N_I = 0.154$ (at $E = 3$ MeV/nucleon) and $N_I = 0.689$ (at $E = 41.6$ MeV/nucleon) from our work mentioned previously and obtained by a fitting procedure are in a correct “direction” and they are between the estimations using Refs. [43] and [44].

We note that these estimations are valid only for the volume OPs (even in the local density approximation). We emphasize that one has to account also for the competition with the channels at the nuclear periphery (the breakup) that, according to the coupled-channel calculations, play an important role. Their contribution that had been initially obtained only accounting for the channels of NN scattering

inside the nuclear matter leads to changes of the ImOP in the elastic channel. An example for such a “renormalization” of ImOP for elastic $d + A$ scattering from the stripping channel was given in Ref. [45]. For more complex systems this is difficult to be done because only in the (d, p) reaction one can use the approximation of the “delta” potential in the deuteron. Thus, we note that not only the Pauli blocking, but also other processes from different mechanisms (breakup and others) play a role, as it is considered in various references mentioned in Sec. I of the present work.

IV. SUMMARY AND CONCLUSIONS

The results of the present work can be summarized as follows:

- (i) The microscopic optical potential and cross sections of ${}^6\text{He} + {}^{12}\text{C}$ elastic scattering were calculated at the energies of $E = 3, 38.3, \text{ and } 41.6$ MeV/nucleon. Comparisons with the experimental data and results of other approaches were presented. The direct and exchange parts of the real OP (V^{DF}) were calculated microscopically using the double-folding procedure and density-dependent M3Y (of CDM3Y6-type) effective interaction based on the Paris nucleon-nucleon potential. The imaginary parts of the OP were taken in the forms of V^{DF} or W^H , the latter being calculated using the high-energy approximation. The microscopic densities of protons and neutrons in ${}^6\text{He}$ calculated within the large-scale shell model were used. The nucleon density distribution functions of ${}^{12}\text{C}$ were taken as defolded charged densities obtained from the best fit to the experimental form factors from electron elastic scattering on ${}^{12}\text{C}$. In this way, in contrast to the phenomenological and semi-microscopic models we deal with a fully microscopic approach as a physical ground to account for the single-particle structure of the colliding nuclei. The elastic scattering differential cross sections were calculated using the program DWUCK4.
- (ii) Although at low energies the volume OPs can reproduce sufficiently well the experimental data, at higher energies additional surface terms in the OP having a form of a derivative of the imaginary part of the OP became necessary and were used in the present work.
- (iii) The depths of the real and imaginary parts of the microscopic OPs are considered as fitting parameters. As is expected when one utilizes the fitting procedure in the case of a limited number of experimental data, the

problem of the ambiguity of these parameters arises. To overcome (at least partly) this ambiguity, additional physical constraints should be imposed. Doing so, we require in our work the values of the depth’s N parameters to lead to volume integrals J_V and J_W with realistic energy dependence for energies $0 < E < 100$ MeV/nucleon. Namely, J_V ’s must decrease while J_W ’s increase to some constant values with the increase of the energy.

- (iv) The comparison of our results with those of some phenomenological approaches pointed out the advantages of using microscopic real and imaginary parts of the optical potential imposing realistic physical constraints on their depths, e.g. the behavior of the volume integrals as functions of the energy.
- (v) As in works of other authors (e.g., Ref. [5]) we consider in more details the behavior of the OP in the nuclear periphery. This gives us the possibility of making some conclusions about the contributions of the dynamical polarization terms of the OP or, in other words, about the coupled-channel effects.
- (vi) It is shown that the deviations of the N values from unity (given in Table I for the volume OPs) that are obtained by a fit to the experimental data for ${}^6\text{He} + {}^{12}\text{C}$ elastic scattering are related to the Pauli blocking effects. These values are smaller than unity and turn out to be between the approximate estimations performed using the results of approaches where Pauli blocking is taken into account (e.g., Refs. [43,44]). It is also mentioned that together with the important Pauli blocking effects, the role of other mechanisms, such as breakup processes, also have to be accounted for in the study of the reaction considered.

ACKNOWLEDGMENTS

The work is partly supported by the Agreement for Cooperation between the Institute for Nuclear Research and Nuclear Energy of the Bulgarian Academy of Sciences (Sofia) and Joint Institute for Nuclear Research (Dubna). Three of the authors (D.N.K., A.N.A., and M.K.G.) are grateful for the support of the Bulgarian Science Fund under Contract No. 02–285, and one of them (D.N.K.) under Contract No. DID–02/16–17.12.2009. The authors E.V.Z. and K.V.L. thank the Russian Foundation for Basic Research (Grant No. 09-01-00770) for partial support.

[1] N. Keeley, N. Alamanos, K. W. Kemper, and K. Rusek, *Prog. Part. Nucl. Phys.* **63**, 396 (2009).
 [2] K. Amos, W. A. Richter, S. Karataglidis, and B. A. Brown, *Phys. Rev. Lett.* **96**, 032503 (2006); P. K. Deb, B. C. Clark, S. Hama, K. Amos, S. Karataglidis, and E. D. Cooper, *Phys. Rev. C* **72**, 014608 (2005).
 [3] M. Avrigeanu, G. S. Anagnostatos, A. N. Antonov, and J. Giapitzakis, *Phys. Rev. C* **62**, 017001 (2000); M. Avrigeanu,

G. S. Anagnostatos, A. N. Antonov, and V. Avrigeanu, *Int. J. Mod. Phys. E* **11**, 249 (2002).
 [4] G. R. Satchler and W. G. Love, *Phys. Rep.* **55**, 183 (1979); G. R. Satchler, *Direct Nuclear Reactions* (Clarendon, Oxford, 1983).
 [5] D. T. Khoa and W. von Oertzen, *Phys. Lett. B* **304**, 8 (1993); **342**, 6 (1995); D. T. Khoa, W. von Oertzen, and H. G. Bohlen, *Phys. Rev. C* **49**, 1652 (1994); D. T. Khoa, W. von Oertzen, and A. A. Ogloblin, *Nucl. Phys. A* **602**, 98 (1996); Dao T. Khoa

- and Hoang Sy Than, *Phys. Rev. C* **71**, 044601 (2005); O. M. Knyaz'kov, *Sov. J. Part. Nuclei* **17**, 137 (1986).
- [6] D. T. Khoa and G. R. Satchler, *Nucl. Phys. A* **668**, 3 (2000); D. T. Khoa, G. R. Satchler, and W. von Oertzen, *Phys. Rev. C* **56**, 954 (1997).
- [7] S. Karataglidis, P. J. Dortmans, K. Amos, and C. Bennhold, *Phys. Rev. C* **61**, 024319 (2000).
- [8] K. V. Lukyanov, V. K. Lukyanov, E. V. Zemlyanaya, A. N. Antonov, and M. K. Gaidarov, *Eur. Phys. J. A* **33**, 389 (2007).
- [9] V. K. Lukyanov, E. V. Zemlyanaya, K. V. Lukyanov, D. N. Kadrev, A. N. Antonov, M. K. Gaidarov, and S. E. Massen, *Phys. Rev. C* **80**, 024609 (2009).
- [10] K. V. Lukyanov, E. V. Zemlyanaya, and V. K. Lukyanov, *Comm. JINR Preprint P4-2004-115*, Dubna (2004); *Phys. At. Nucl.* **69**, 240 (2006).
- [11] P. Shukla, *Phys. Rev. C* **67**, 054607 (2003).
- [12] R. J. Glauber, *Lectures in Theoretical Physics*, edited by W. E. Britten and L. G. Dunham (Interscience Publishers, New York, 1959), Vol. 1, p. 315.
- [13] A. G. Sitenko, *Ukr. Phys. J.* **4**, 152 (1959).
- [14] W. Czyz and L. C. Maximon, *Ann. Phys.* **52**, 59 (1969); J. Formanek, *Nucl. Phys. B* **12**, 441 (1969).
- [15] M. Milin *et al.*, *Nucl. Phys. A* **730**, 285 (2004).
- [16] V. Lapoux *et al.*, *Phys. Rev. C* **66**, 034608 (2002).
- [17] J. S. Al Khalili *et al.*, *Phys. Lett. B* **378**, 45 (1996).
- [18] Y. Kucuk, I. Boztosun, and T. Topel, *Phys. Rev. C* **80**, 054602 (2009).
- [19] M. El-Azab Farid, A. M. A. Nossair, and A. A. Ibraheem, *Int. J. Mod. Phys. E* **17**, 715 (2008).
- [20] J. P. Jeukenne, A. Lejeune, and C. Mahaux, *Phys. Rev. C* **16**, 80 (1977).
- [21] B. Abu Ibrahim and Y. Suzuki, *Nucl. Phys. A* **728**, 118 (2003); *Phys. Rev. C* **70**, 011603(R) (2004).
- [22] T. Matsumoto, T. Egami, K. Ogata, Y. Iseri, M. Kamimura, and M. Yahiro, *Int. J. Mod. Phys. A* **24**, 2191 (2009).
- [23] M. V. Zhukov, B. V. Danilin, D. V. Fedorov, J. M. Bang, I. J. Thompson, and J. S. Vaagen, *Phys. Rep.* **231**, 151 (1993).
- [24] J. W. Negele and D. Vautherin, *Phys. Rev. C* **5**, 1472 (1972).
- [25] K. V. Lukyanov, *Comm. JINR*, P11-2007-38, Dubna (2007).
- [26] S. K. Charagi and S. K. Gupta, *Phys. Rev. C* **41**, 1610 (1990); **46**, 1982 (1992).
- [27] P. Shukla, [arXiv:nucl-th/0112039](https://arxiv.org/abs/nucl-th/0112039).
- [28] G. D. Alkhazov, S. L. Belostotsky, and A. A. Vorobyov, *Phys. Rep.* **42**, 89 (1978).
- [29] A. Vitturi and F. Zardi, *Phys. Rev. C* **36**, 1404 (1987).
- [30] D. M. Brink and G. R. Satchler, *J. Phys. G* **7**, 43 (1981).
- [31] V. Lapoux *et al.*, *Phys. Lett. B* **517**, 18 (2001).
- [32] D. T. Khoa, G. R. Satchler, and W. von Oertzen, *Phys. Lett. B* **358**, 14 (1995).
- [33] M. Hussein and G. R. Satchler, *Nucl. Phys. A* **567**, 165 (1994).
- [34] V. K. Lukyanov, E. V. Zemlyanaya, and B. Słowiński, *Phys. At. Nucl.* **67**, 1282 (2004).
- [35] V. V. Burov and V. K. Lukyanov, *Comm. JINR*, P4-11098, Dubna (1977); V. V. Burov, D. N. Kadrev, V. K. Lukyanov, and Yu. S. Pol', *Phys. At. Nucl.* **61**, 595 (1998).
- [36] P. D. Kunz and E. Rost, in *Computational Nuclear Physics*, edited by K. Langanke *et al.* (Springer-Verlag, New York, 1993), Vol. 2, p. 88.
- [37] A. N. Tikhonov and V. Y. Arsenin, *Solutions of Ill-Posed Problems* (V. H. Winston and Sons/Wiley, New York, 1977).
- [38] E. A. Romanovsky *et al.*, *Bull. Rus. Acad. Sci., Phys.* **62**, 150 (1998).
- [39] C. Mahaux and H. Ngo, *Nucl. Phys. A* **378**, 205 (1982).
- [40] M. E. Brandan and G. R. Satchler, *Phys. Rep.* **285**, 143 (1997).
- [41] M. S. Hussein, R. A. Rego, and C. A. Bertulani, *Phys. Rep.* **201**, 279 (1991).
- [42] G. Q. Li and R. Machleidt, *Phys. Rev. C* **48**, 1702 (1993); **49**, 566 (1994).
- [43] C. Xiangzhou, F. Jun, S. Wenqing, M. Yugang, W. Jiansong, and Y. Wei, *Phys. Rev. C* **58**, 572 (1998).
- [44] C. A. Bertulani and C. De Conti, [arXiv:1004.2096](https://arxiv.org/abs/1004.2096) [nucl-th]; *Phys. Rev. C* **81**, 064603 (2010).
- [45] A. Ingemarsson and R. Shyam, *Phys. Rev. C* **60**, 054615 (1999).